

Effect of the isotropic collisions with neutral hydrogen on the polarization of the CN solar molecule

S. Qutub¹, M. Derouich^{1,2*}, Y.N. Kalugina^{3,4}, H. Assiri¹, F. Lique⁵

¹ *Astronomy Dept, Faculty of Science, King Abdulaziz University, Jeddah, Saudi Arabia*

² *Sousse University, ESSTHS, Lamine Abbassi street, 4011 H. Sousse, Tunisia*

³ *Department of Optics and Spectroscopy, Tomsk State University, 36 Lenin av., Tomsk 634050, Russia*

⁴ *Institute of Spectroscopy, Russian Academy of Sciences, Fizicheskaya St. 5, 108840 Troitsk, Moscow, Russia*

⁵ *LOMC - UMR 6294, CNRS-Université du Havre, 25 rue P. Lebon, BP 1123, F-76063 Le Havre, France*

Accepted 2019 October 22. Received 2019 September 22; in original form 2019 July 04

ABSTRACT

Our work is concerned with the case of the solar molecule CN which presents conspicuous profiles of scattering polarization. We start by calculating accurate PES for the singlet and triplet electronic ground states in order to characterize the collisions between the CN molecule in its $X^2\Sigma$ state and the hydrogen in its ground state 2S . The PES are included in the Schrödinger equation to obtain the scattering matrix and the probabilities of collisions. Depolarizing collisional rate coefficients are computed in the framework of the infinite order sudden approximation for temperatures ranging from $T = 2000$ K to $T = 15000$ K. Interpretation of the results and comparison between singlet and triplet collisional rate coefficients are detailed. We show that, for typical photospheric hydrogen density ($n_H = 10^{15} - 10^{16} \text{ cm}^{-3}$), the $X^2\Sigma$ state of CN is partially or completely depolarized by isotropic collisions.

Key words: Collisions – Sun: photosphere – atomic processes – line: formation - polarization

1 INTRODUCTION

Observations of linear polarization close to the solar limb have revealed the existence, in the second solar spectrum (SSS), of prominent linear polarization signals due to molecular

* derouichmoncef@gmail.com

lines (e.g. Mohan Rao and Rangarajan 1999; Gandorfer 2000; Faurobert & Arnaud 2003; Berdyugina & Fluri 2004; Asensio Ramos & Trujillo Bueno 2005; Milić & Faurobert 2012). In particular, the CN molecule, which shows weak lines in the usual (unpolarized) solar spectrum, presents conspicuous peaks in the SSS (Shapiro et al. 2011). The SSS is the observational signature of the polarization of the CN rotational levels which consists on population imbalances and quantum coherences among their Zeeman sub-levels.

In the solar photosphere, polarized CN levels undergo the effect of isotropic collisions between emitting or absorbing molecules and nearby hydrogen atoms. Since collisions are isotropic, they tend to partially or totally destroy the polarization of CN lines. In addition, the Hanle effect of a solar magnetic field results in a partial decrease of the polarization of the CN states. Thus, the depolarizing effects of the isotropic collisions and the Hanle effect are mixed in the same observable (the polarization state), which makes the interpretation of the observed polarization in terms of magnetic fields complicated because of the almost complete lack of collisional molecular depolarization rates. To derive magnetic fields from the interpretation of the SSS, it is fundamental to firstly determine the depolarizing collisional rate coefficients, and then to include these data in the formalism of the formation of the polarized lines.

Over more than 40 years, vigorous efforts were concerned with the calculation of the collisional ro-vibrational (de)excitation rates for interstellar molecules (e.g. Roueff & Lique 2013). The majority of the works were dedicated to the modelling of the molecular line profiles. The effect of the collisional excitation on the molecular polarization profiles is usually overlooked. The literature in argument, there are no calculations of depolarization rates for solar molecular lines by collisions with neutral hydrogen.

Our intention in this work is to provide new (de)polarization collisional rates for the CN molecule in its ground state $X^2\Sigma$ which is very important in the solar polarization studies. Computations of collisional rates occur in two steps. The first step is the determination of potential energy surfaces (PES) in order to characterize the interactions between the atom and the molecule. All the PES were obtained using the MOLPRO package (e.g. Werner et al. 2010). The second step is the study of the dynamics of collisions by solving the Schrödinger equation. Dynamics calculations are made possible thanks to the MOLSCAT code (Hutson & Green 1994). The depolarization cross-sections have been computed within the infinite-order-sudden (IOS) approximation for first 40 rotational levels and for kinetic

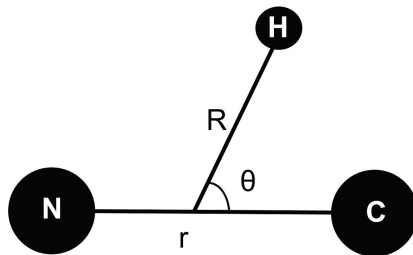


Figure 1. Coordinate system of the CN – H interaction.

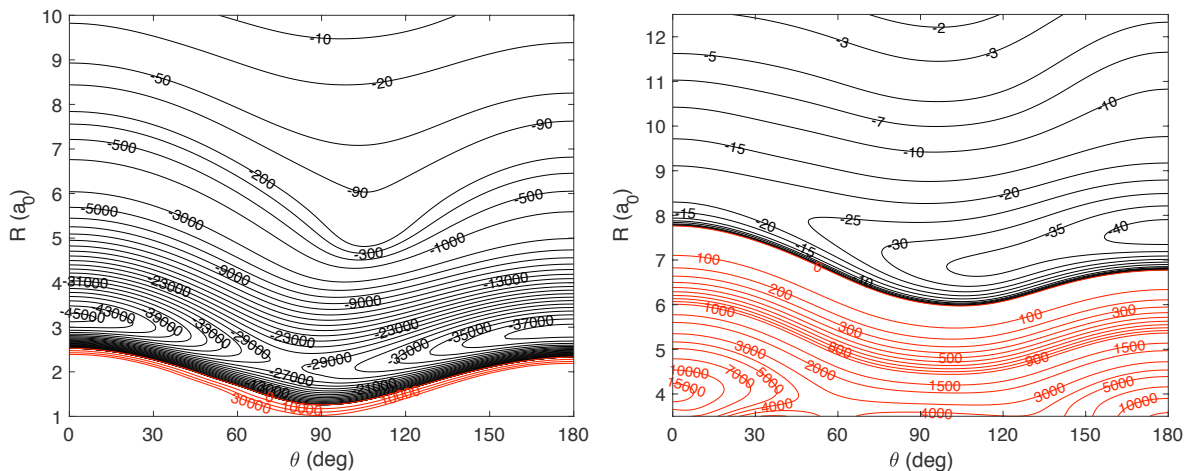


Figure 2. 2D potential energy surface for singlet state (left panel) and triplet state (right panel). Energy is in cm^{-1} .

energies ranging from 400 to 20000 cm^{-1} . This allowed us to calculate depolarization rates of the state $X^2\Sigma$ of the CN for temperatures between 2000 and 15000 K.

2 POTENTIAL ENERGY SURFACES

In the present work, the coordinate system presented in Fig. 1 was used. The center of coordinates coincides with the center of mass of the CN molecule. Intermolecular vector R connects the centre of mass of CN molecule and H atom. Angle θ defines the rotation of the hydrogen atom around the CN molecule. Thus, the mutual orientation and position of the H atom is described by the intermolecular separation, R , and by angle θ .

The CN molecule is assumed rigid with geometrical structure corresponding to the equilibrium: $r = 2.2144 a_0$ (e.g. Yang et al. 2016).

When CN molecule in the ground electronic state $2\Sigma^+$ interacts with the hydrogen atom in $2S$ ground electronic state the system can exist in two electronic states with total electronic spin $\vec{S}_t = \vec{S}_{CN} + \vec{S}_H$. Thus, we have to obtain the potential energy surfaces for the singlet (1A) and triplet (3A) states.

Ab initio calculations of the PES for the singlet and triplet electronic states of CN – H were carried out at multireference internally contracted configuration interaction (MRCI) (Werner 1988) level of theory. The size consistency was partially corrected using the Davidson (+Q) correction (Davidson 1977), the rest was corrected by subtracting the energy at $R=100 a_0$. The 1s core electrons of the Nitrogen and Carbon atoms were kept frozen. The active space consists of 10 electrons distributed in the 9 orbitals. The augmented correlation-consistent triple zeta (aVTZ) basis set (Dunning 1989) augmented by (3s, 2p, 1d) mid-bond functions (bf) (Williams et al. 1995) were used. The computations were performed using MOLPRO 2010 package (e.g. Werner et al. 2010).

For the singlet electronic state the intermolecular distance was varied from 1 to 60 a_0 giving 45 grid points. For the triplet electronic state the R values were varied from 3.5 to 60 a_0 with total of 35 grid points. The angle θ was varied from 0° to 180° with a step of 5° . Due to high anisotropy of the 1A potential the 2D-spline was employed for the representation of both PESs at any set (R, θ) . The resulting potential energy surfaces for the singlet and triplet electronic states are presented in Fig. 2.

There are two minima on the PES for the singlet state corresponding to the formation of HCN and HNC molecules. The HCN arrangement corresponds to the minimal structure with $\theta = 0^\circ$ and $R = 3.2 a_0$ and has the well depth $E = -45426 \text{ cm}^{-1}$. The HNC minimal structure corresponds to $\theta = 180^\circ$ and $R = 2.92 a_0$ and has a well depth $E = -40098 \text{ cm}^{-1}$. The minimum for the triplet state occurs at $R = 7.6 a_0$, $\theta = 180^\circ$ and has an energy $E = -42.40 \text{ cm}^{-1}$.

In Figure 3, we respectively show 3-dimensional plots of singlet and triplet components of the potential energy for the CN-H system.

3 THEORETICAL BACKGROUND

3.1 Basis of irreducible tensorial operators

Physical interpretation of the solar polarization requires suitable description of the internal states of the emitting/absorbing molecules with the density matrix formalism expressed on the basis of irreducible tensorial operators (e.g. Sahal-Br  chot 1977; Trujillo Bueno 2002; Landi Degl’Innocenti & Landolfi 2004). The CN states are described by the density matrix elements $\rho_q^k(j)$ where j is the molecular angular momentum, k is the tensorial order ($0 \leq k \leq 2j$) and q quantifies the coherence between the sublevels ($-k \leq q \leq k$). The circular

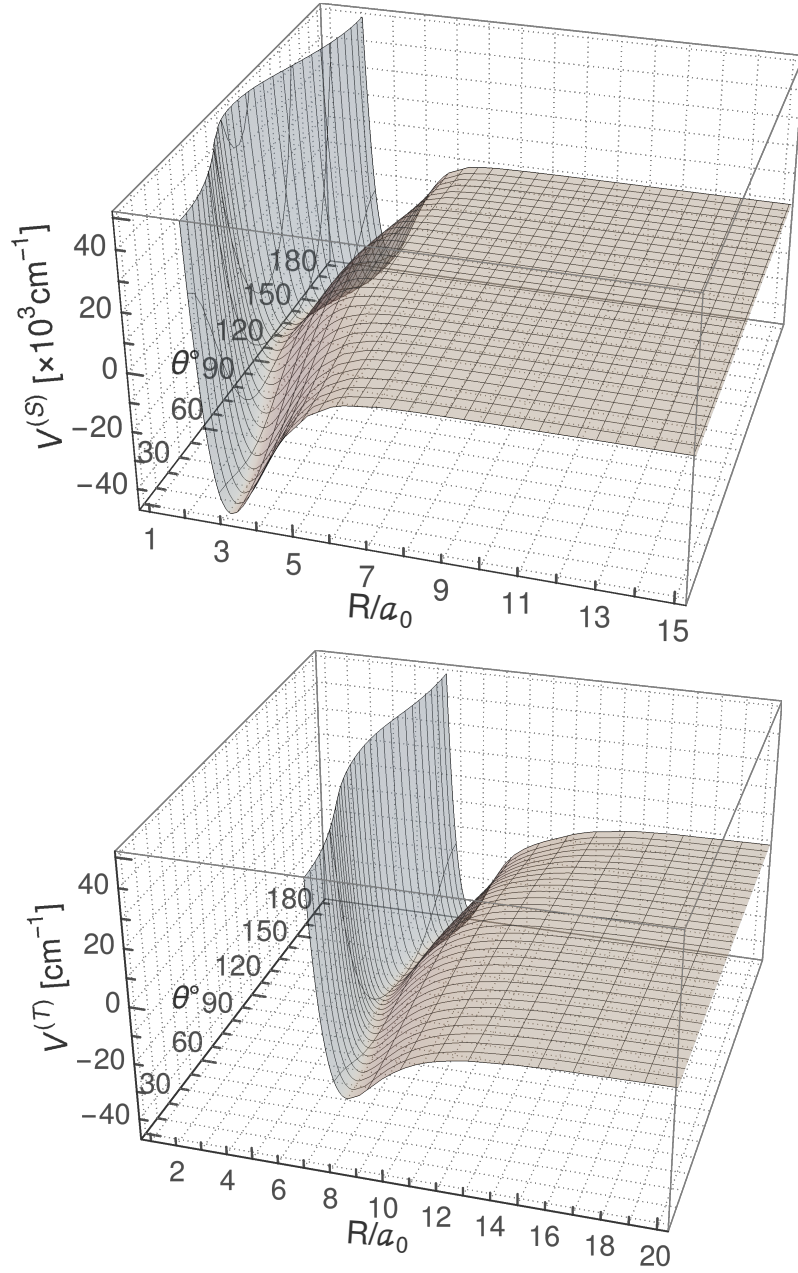


Figure 3. 3D plots of the singlet, $V^{(S)}$, and triplet, $V^{(T)}$, components of the CN-H potential, respectively.

polarization of the molecule is quantified by the density matrix elements with odd k ($j\rho_q^{k=1}$, $j\rho_q^{k=3}$, etc.), while the linear polarization is quantified with the even ones: $j\rho_q^{k=2}$, $j\rho_q^{k=4}$, etc. The intensity of the transition involving the j -level is given by the density matrix element $j\rho_q^{k=0}$. In order to study the SSS, one has to calculate the density matrix elements with even tensorial orders $k=0, 2, 4$, etc. In addition, it is to be noticed that $j\rho_q^{k=0}$ is proportional to the j -level population.

In studies concerned with the analysis of only the intensity spectrum of the light, only the element $j\rho_q^{k=0}$ is the unknown to be determined and one needs solely the collisional

rates with $k = 0$. These rates are similar to the usual collisional excitation rates which are typically calculated and included in the radiative transfer codes synthesising the ordinary intensity profiles. Rates with $k \geq 0$ are needed for the cases of spectropolarimetric studies, i.e. where the goal is to synthesise not only the intensity profiles but also the polarization profiles. One needs to adopt a formalism treating the interaction between an open-shell systems which takes in consideration the cases where $k > 0$ corresponding to the effect of the collisions on the polarized light. Note that the isotropy of the velocity distribution of the hydrogen atoms implies that the polarization transfer rates are q -independent (e.g. Sahal-Br  chot 1977; Derouich et al. 2003; Derouich et al. 2007).

3.2 Coupling scheme approach

We are interested in the electronic $^2\Sigma^+$ state of the CN solar molecule. The CN levels can be described in the Hund's case (b) limit. The fine structure levels are labeled by N and j , where N is the rotational angular momentum and j the total molecular angular momentum given by $j = N + S_d$ where $S_d = 1/2$ represents the spin of CN in its $^2\Sigma^+$ state. Thus, $j = N \pm 1/2$. CN molecule in the $^2\Sigma^+$ state collides with hydrogen atom in its ground state 2S . The spin of the hydrogen is $S_a = 1/2$, thus the collision results in producing a singlet state $^1A'$ with total spin $S_t = 0$ and a triplet state $^3A'$ with $S_t = 1$.

Corey & Alexander (1985) and Corey et al. (1986) have studied the general case concerned with cross-sections for collisions between open-shell systems; however they did not take into account the effects of the collisions on the molecular polarization. Corey & Alexander (1985) and Corey et al. (1986) found that in the expression of each cross-section contains the effect of different components of the interaction potentials. For instance, the cross-section associated to a singlet state includes not only the singlet component of the interaction potential but also the triplet component, in addition to an interference term arising from the open-shell nature of both colliding systems. Corey & Alexander (1985) and Corey et al. (1986) showed that, in the infinite-order-sudden (IOS) approximation, the excitation cross-sections can be written as a linear combination of IOS cross-sections (see also Goldflam et al. 1977). Interestingly, in the expression of the IOS cross-section one has also to take into account the contribution of interaction potentials with different spin values.

We follow the formalism presented in Corey & Alexander (1985) and Corey et al. (1986), and we apply it to obtain the expression of the polarization transfer and depolarization

cross-sections $\sigma^k(Nj \rightarrow N'j')$ due to the isotropic collisions between the CN molecule with an open-shell perturber like the hydrogen. We adopt the IOS approximation which can be well justified especially for sufficiently high temperatures (see e.g. Lique et al. 2007). In fact, as we are interested in the solar context, where the temperatures and the kinetic energies of collisions are high, one can expect that some simplification regarding the coupling effects should be invoked in order to obtain results with acceptable accuracy in reasonable computing time. Let us notice also that this is the first work which is intended to determine depolarization rates by collisions between a molecule in an open shell state and the hydrogen atom in its open shell ground state. Our approximate approach can be summarized by the following indications:

- We start by precisely calculating the interaction potentials associated to the singlet $^1A'$ with total spin $S_t = 0$ and the triplet state $^3A'$ with $S_t = 1$.
- Then, the Schrödinger equation describing the dynamics of collisions is solved for each potential to obtain the corresponding singlet and triplet IOS cross-sections $\sigma(0 \rightarrow L)$.
- In these conditions, for each value of the total spin, we assume that the depolarization cross-sections for a tensorial order k are given by the same expression established previously in the case of an openshell molecule with a spinless atom. This assumption allows us to factorize the $\sigma^k(Nj \rightarrow N'j')$ into a product of terms involving the geometrical factors and coupling scheme effects and a term given as a linear combination of the IOS cross-sections $\sigma(0 \rightarrow L)$ (e.g. Corey & Smith 1985):

$$\begin{aligned} \sigma^k(Nj \rightarrow N'j') = \sum_L (-1)^{k+L+j+j'+1} & \begin{Bmatrix} j & j' & L \\ j' & j & k \end{Bmatrix} \\ (2N+1)(2N'+1)(2j'+1)(2j+1) \times & \begin{Bmatrix} N & N' & L \\ j' & j & S_a \end{Bmatrix}^2 \\ & \begin{pmatrix} N' & N & L \\ 0 & 0 & 0 \end{pmatrix}^2 \sigma(0 \rightarrow L). \end{aligned} \quad (1)$$

The depolarization cross-sections are defined by (e.g. Derouich et al. 2003; Landi Degl'Innocenti & Landolfi 2004, Dagdigian & Alexander 2009):

$$\sigma^k(Nj) = \sigma^0(Nj \rightarrow Nj) - \sigma^k(Nj \rightarrow Nj). \quad (2)$$

In order to obtain the total cross-section averaged over the spin one has:

$$\sigma^k(Nj \rightarrow N'j') = \frac{1}{4} \times [3 \times \sigma^k(Nj \rightarrow N'j'; ^3A') + \sigma^k(Nj \rightarrow N'j'; ^1A')]. \quad (3)$$

The depolarization rates, $D^k(Nj, T)$, of the level (Nj) due to elastic collisions and the polarization transfer rates, $D^k(Nj \rightarrow v'N'j', T)$, between the levels Nj and $v'N'j'$ are given by integration over Maxwellian distribution of relative kinetic energies (or relative velocities). In addition,

$$D^k(Nj) = D^0(Nj \rightarrow Nj) - D^k(Nj \rightarrow Nj) \quad (4)$$

which means that $D^0(Nj) = 0$ by definition.

If $S_d = S_t=0$, thus $j = N$, $j' = N'$, and $j + j' = N + N'$ is even, one can demonstrate that (e.g. Derouich 2006; Lique et al. 2007):

$$\sigma^k(Nj \rightarrow N'j') = \sigma^k(j \rightarrow j') = \sum_{L>0}^{j+j'} (-1)^k (2j'+1)(2j+1) \begin{Bmatrix} j' & j' & k \\ j & j & L \end{Bmatrix} \left(\begin{matrix} j & L & j' \\ 0 & 0 & 0 \end{matrix} \right)^2 \sigma(v0 \rightarrow vL) \quad (5)$$

and in the case where $k = 0$, one finds (e.g. Derouich 2006):

$$\sigma^0(Nj \rightarrow N'j') = \sqrt{\frac{2j+1}{2j'+1}} \sigma(Nj \rightarrow N'j'). \quad (6)$$

3.3 Statistical equilibrium equations

Physical interpretation of the observed polarization requires the solution of the coupling between polarized radiative transfer in the solar atmosphere and statistical equilibrium equations. In such situation, description of the internal states of the emitting/absorbing molecule in the density matrix formalism expressed on the basis of irreducible tensorial operators is shown as a most suitable (e.g. Sahal-Br echot 1977; Landi Degl'Innocenti & Landolfi 2004).

The contribution of the isotropic collisions to the statistical equilibrium equations is:

$$\begin{aligned} \left(\frac{d^j \rho_q^k}{dt} \right)_{coll} &= -D^k(j, T) {}^j \rho_q^k \\ &\quad - {}^j \rho_q^k \sum_{j' \neq j} \sqrt{\frac{2j'+1}{2j+1}} D^0(j \rightarrow j', T) \\ &\quad + \sum_{j' \neq j} D^k(j' \rightarrow j, T) {}^{vj'} \rho_q^k \end{aligned} \quad (7)$$

The quantities to be computed are the density matrix elements ${}^j \rho_q^k$.

$D^k(j, T)$ and $D^k(j' \rightarrow j, T)$ should be calculated independently to enter the statistical equilibrium equations. It is to be noticed that, in the solar physical conditions, the polarization transfer rates for vibrational relaxation are smaller than these for pure rotational

relaxation by about three orders of magnitude. Therefore, it is convenient to neglect the effect of the transfer of polarization between different vibrational states.

4 RESULTS AND DISCUSSIONS

We separately feed the singlet and triplet parts of the potential into MOLSCAT code which determines the dynamics of the colliding system by solving the corresponding Schrödinger equation and returns the scattering matrix and cross-sections. To obtain the depolarization and transfer of polarization rates, we thermally average the resultant cross-sections over the kinetic energy distributions of the colliding partners for temperatures ranging from 2000 K to 15000 K using the relations (see e.g. Flower 2003),

$$\langle \sigma^k \nu \rangle = \left(\frac{8}{\pi \mu k_B^3 T^3} \right)^{1/2} \int_0^\infty \sigma^k(E) \exp\left(-\frac{E}{k_B T}\right) E dE, \quad (8)$$

where E is the kinetic energy of the incident atom with respect to the upper level and μ is the reduced mass of the colliding system. For this purpose, we consider collision energies ranging from 400 cm^{-1} to 20000 cm^{-1} . For energies larger than 20000 cm^{-1} , we extrapolate the cross-sections as their variation with energy becomes almost linear for sufficiently large energies. We then calculate the singlet and triplet contributions to the transfer of polarization and depolarization rates using Eqs. 1, 2 and 4. The results of our calculations are shown in Sections 4.1 and 4.2 below.

4.1 Transfer of polarization cross-sections and rates

In Figure 4, we show the energy variation of the upward (upper panels) and downward (lower panels) transfer of polarization cross-sections for the rotational level $N_j = 5_{5.5}$. The contributions of the singlet and triplet parts of the potential are represented by the gray and black curves, respectively. We remark that the cross-sections decrease as k increases. Further, the upward (excitation) and the downward (de-excitation) transfer cross-sections with the same $|\Delta N| = |N' - N|$ from a given level have a very similar behavior; however the upward transfer cross-sections are slightly larger than the downward ones. The difference between the two increases with increasing $|\Delta N|$. Furthermore, we notice that the size of the singlet and triplet contributions to the transfer of polarization cross-sections tends to alternate as $|\Delta N|$ increases.

Let us now consider the thermal average of the transfer of polarization cross-sections, i.e. the rates of transfer of polarization, to study their dependence on temperature and angular

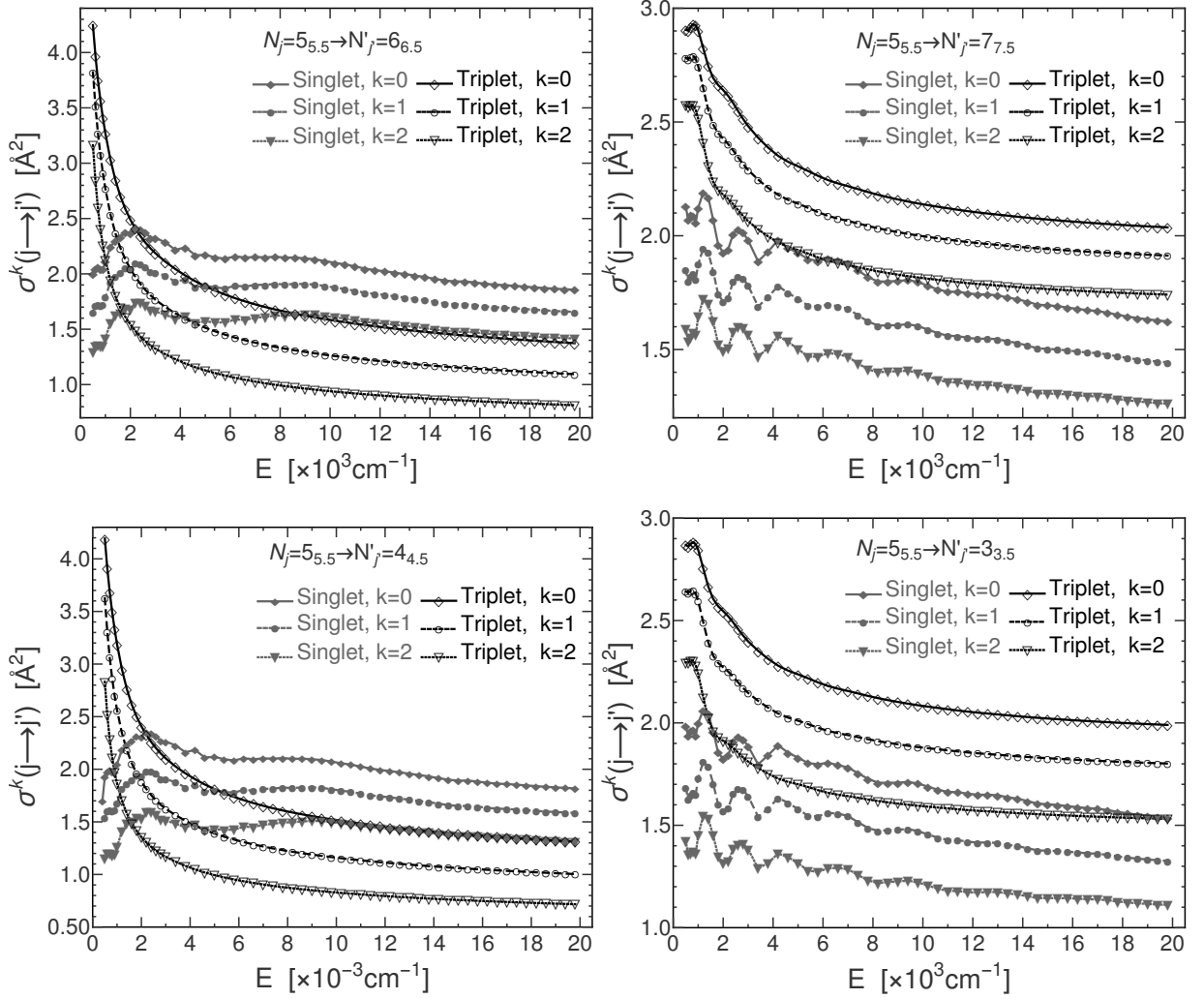


Figure 4. Variation of the upward (upper panels) and downward (lower panels) transfer of polarization cross-sections with energy for the rotational level $N_j = 5_{5.5}$. The singlet and triplet contributions are respectively shown by the gray and black curves for the population, $k = 0$ (diamonds), orientation, $k = 1$ (circles), and alignment, $k = 2$ (down-triangles).

momentum of the rotational levels under consideration. In Figure 5, we show the rates of transfer of polarization as functions of temperature for the levels $N_j = 5_{5.5}$ (upper panels) and $N_j = 10_{10.5}$ (lower panels) in the temperature range $T = 2000 - 15000$ K. It is clear that in the temperature range considered, all rates monotonically increase with increasing temperature.

In Figure 6, we show the dependence of the upward transfer of polarization rates on the angular momentum of the rotational levels considered, j , for various temperatures and $\Delta j = 1$. The left panels show the singlet contribution, while the right panels show the triplet contribution. It can be seen that all rates increase as j increases. We note here that the behavior of the de-excitation (downward) transfer rates from a given level are similar to

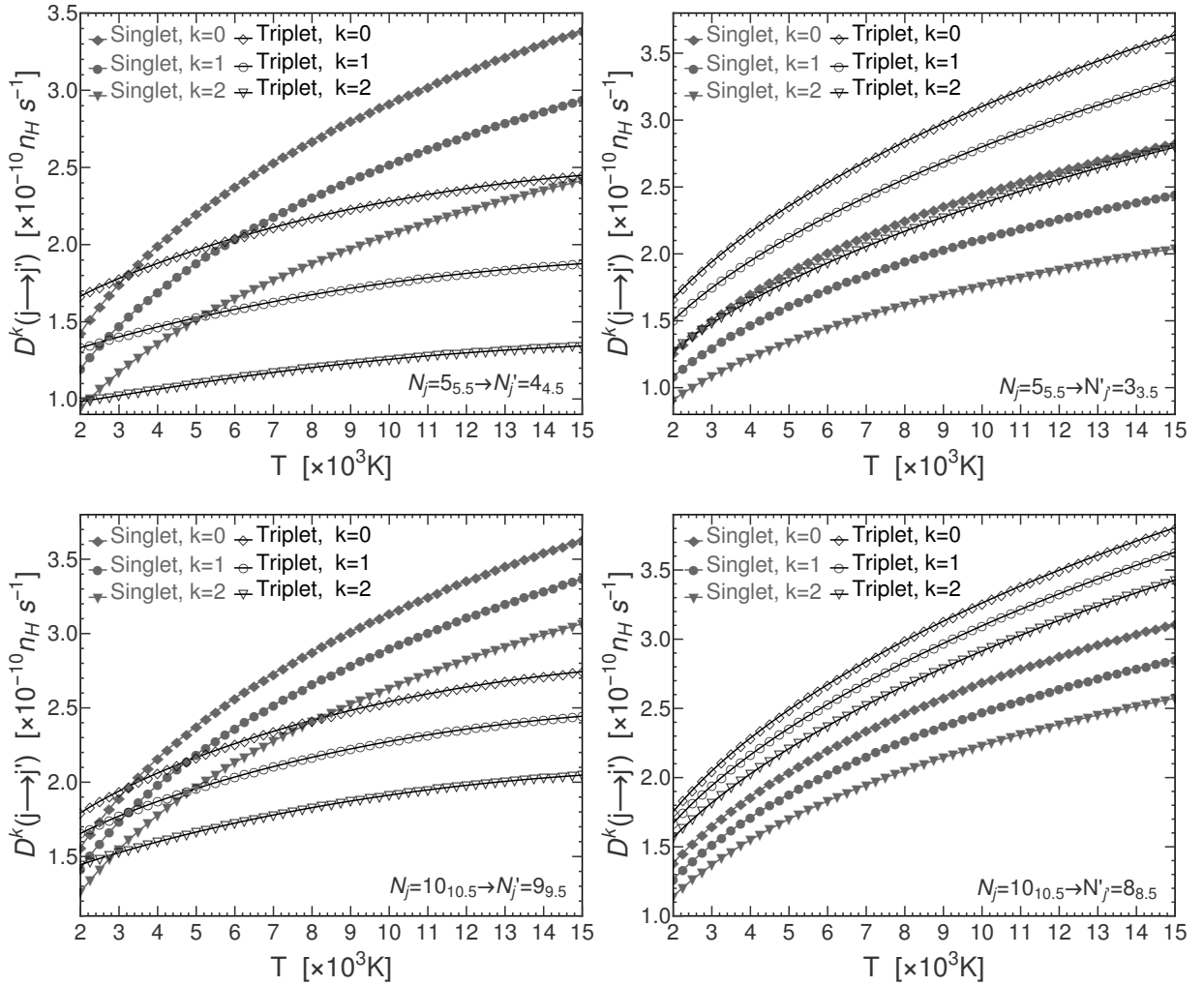


Figure 5. Variation of the singlet (gray curves) and triplet (black curves) contributions to the downward transfer of polarization rates with temperature for the population, $k = 0$ (diamonds), orientation, $k = 1$ (circles), and alignment, $k = 2$ (down-triangles), of the rotational levels $N_j = 5_{5.5}$ (upper panels) and $N_j = 10_{10.5}$ (lower panels).

the upward transfer rates from the same level albeit being a bit lower (see Figure 4 and the discussion relating to it above).

Figure 7 shows the variation with Δj of the singlet (left panel) and triplet (right panel) contributions to the downward transfer of polarization rates for the level $N_j = 10_{10.5}$ at temperature $T = 6000 \text{ K}$. As expected, the rates decrease with increasing Δj . Further, the excitation rates are expected to have behavior with $|\Delta j|$ roughly similar to that of the downward rates. We note here that the singlet and triplet contributions to the transfer of polarization rates are not very different from each other.

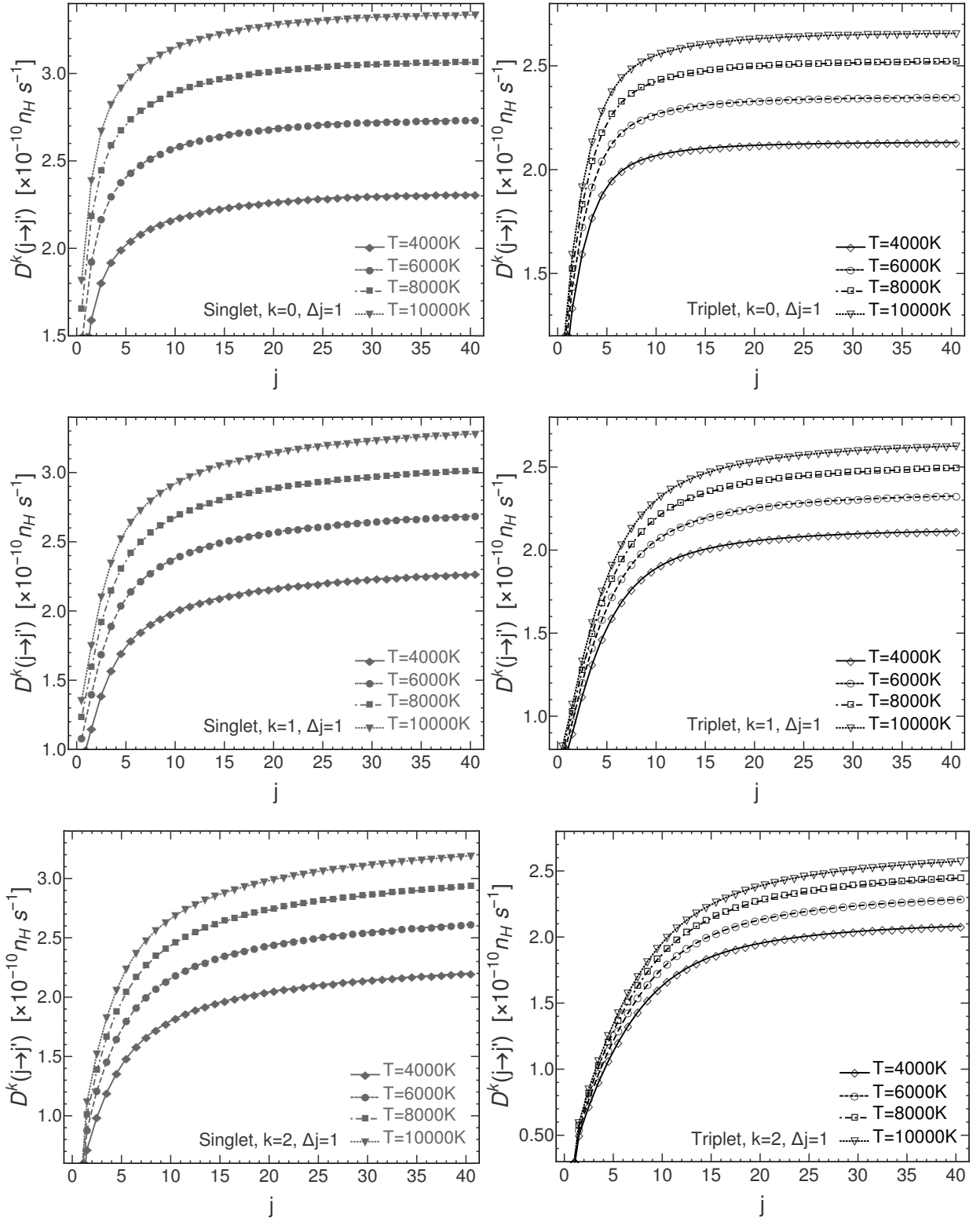


Figure 6. Variation of the upward ($\Delta j = 1$) transfer of polarization rates with j for the singlet (left panels) and triplet (right panels) parts of the potential.

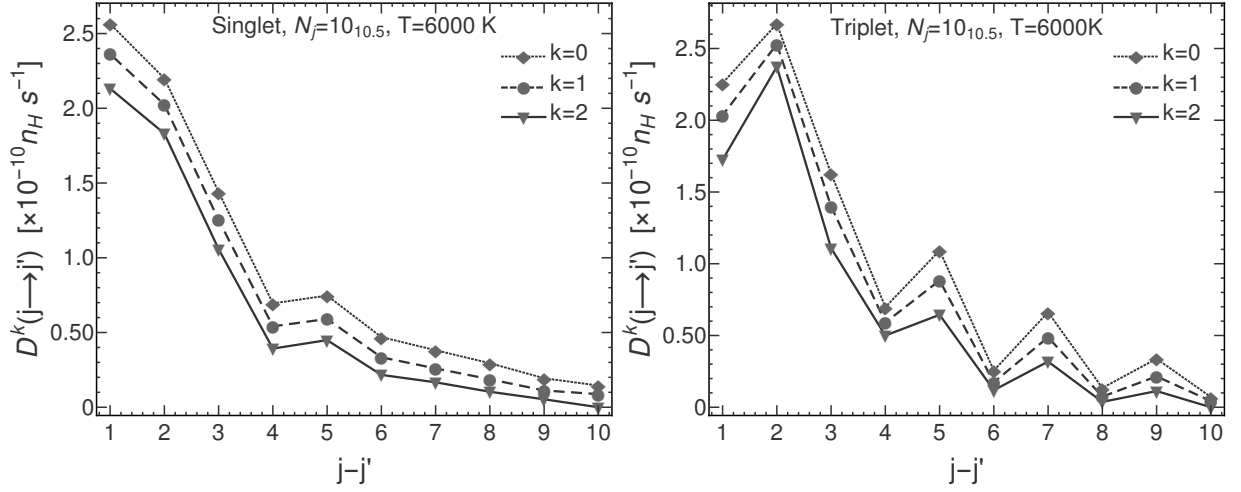


Figure 7. The transfer of polarization rate of the level with $N_j = 10_{10.5}$ as a function of $\Delta j = j - j'$ for the singlet (left panel) and the triplet (right panel) parts of the potential, calculated at temperature $T = 6000\text{K}$.

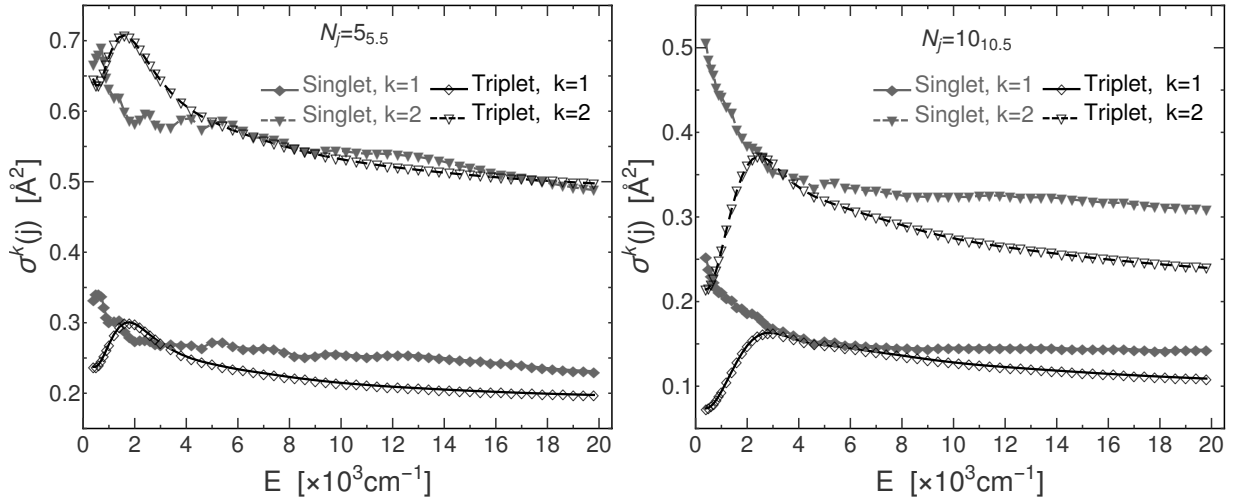


Figure 8. Variation with energy of the depolarization cross-sections of the orientation, $k = 1$ (diamonds), and alignment, $k = 2$ (down-triangles), for the rotational levels $N_j = 5_{5.5}$ (left panel) and $N_j = 10_{10.5}$ (right panel). The singlet and triplet contributions are respectively represented by the gray and black curves.

4.2 Depolarization cross-sections and rates

Let us now turn our attention to the depolarization rates which quantify the destruction of the atomic polarization of a particular level due to purely elastic collisions, i.e. collisions happening inside a given rotational level. Figure 8 shows the depolarization cross-sections for the orientation, $k = 1$ (diamonds), and the alignment, $k = 2$ (down-triangles), of the levels $N_j = 5_{5.5}$ (left panel) and $N_j = 10_{10.5}$ (right panel). One can remark that the cross-sections for the destruction of linear polarization, $\sigma^{k=2}(j)$, is roughly twice as large as that for circular polarization $\sigma^{k=1}(j)$. We next show the dependence of the depolarization rates

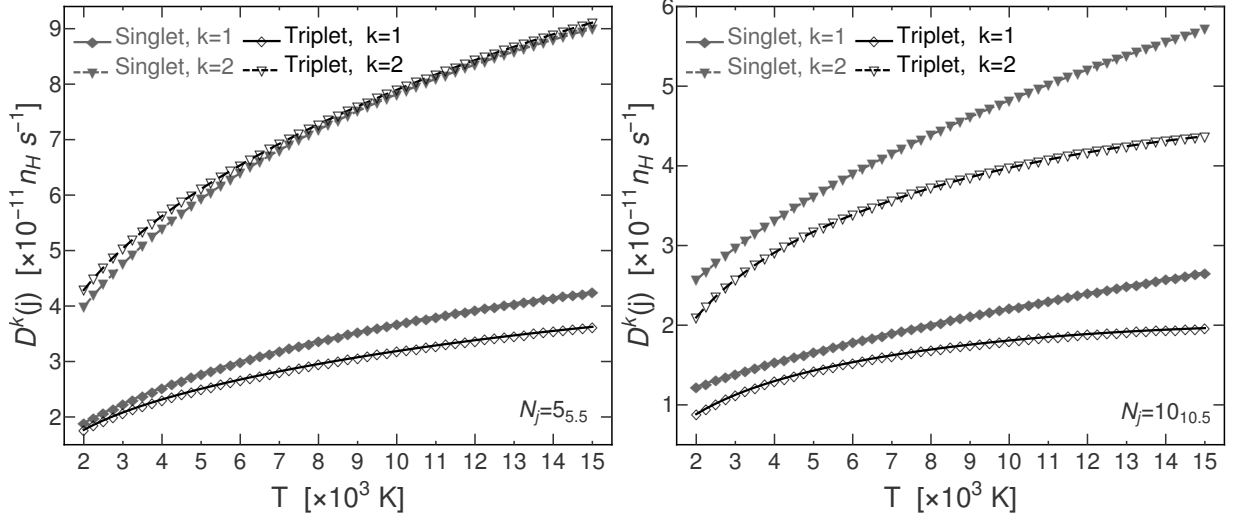


Figure 9. The temperature dependence of the rates of destruction of circular, $k = 1$ (diamonds), and linear, $k = 2$ (down-triangles), polarization for the rotational levels $N_j = 5_{5,5}$ (left panel) and $N_j = 10_{10,5}$ (right panel). The singlet and triplet contributions are respectively represented by the gray and black curves.

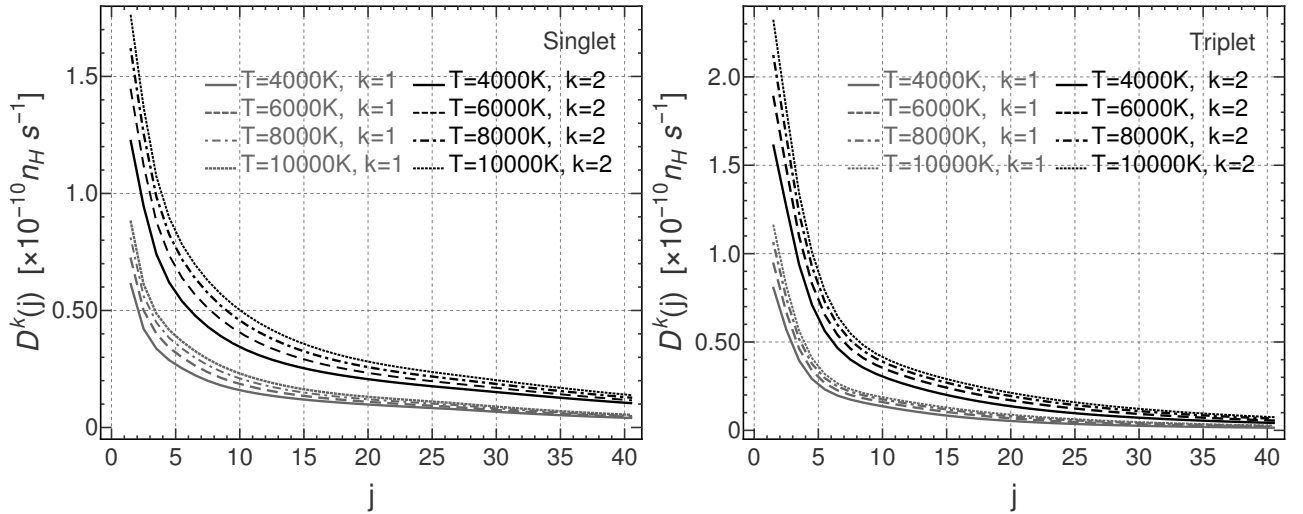


Figure 10. The variation with j of the rates of destruction of circular, $k = 1$, and linear, $k = 2$, polarization of the level N_j for temperatures, $T = 4000, 6000, 8000, 10000$ K. The singlet and triplet contributions are respectively represented by the gray and black curves.

on temperature in Figure 9 for the levels $N_j = 5_{5,5}$ (left panel) and $N_j = 10_{10,5}$ (right panel). As expected, all the rates increase as the temperature increases.

In Figure 10, we show the variation of the depolarization rates with the angular momentum, j , of the levels under consideration for various temperatures. The gray curves represent the singlet contribution, while black curves represent the triplet contribution. Unlike the transfer of polarization rates, the depolarization rates decrease with increasing j . Moreover, the linear depolarization rates are roughly twice as high as the circular depolarization rates. It is interesting to note here that the contribution of the triplet component of the potential

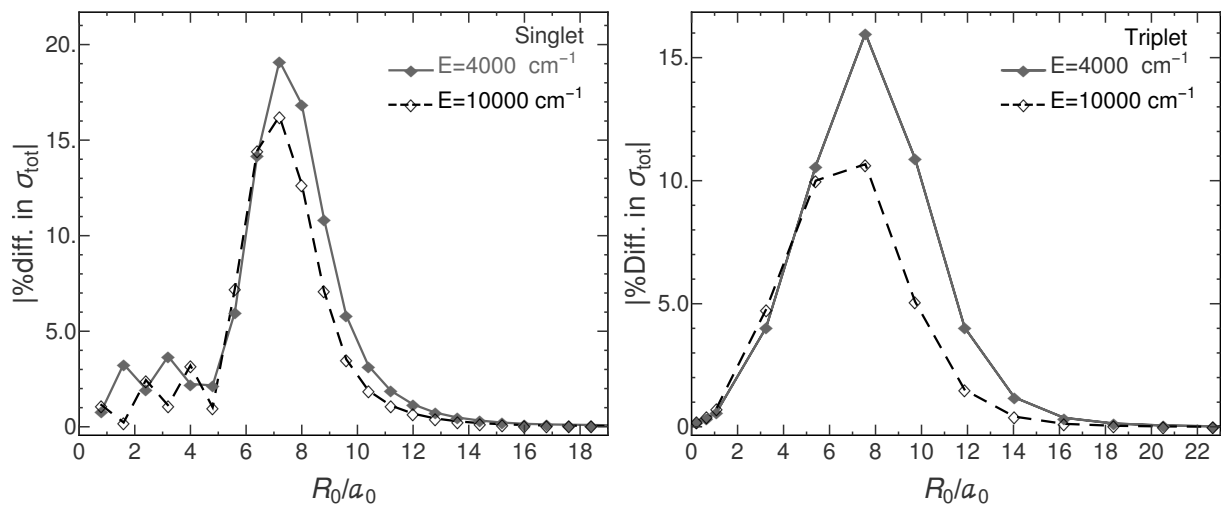


Figure 11. Ratio of the total cross-sections calculated with the perturbed potential to those calculated with the unperturbed potential for collision energy $E = 4000 \text{ cm}^{-1}$ (solid gray lines) and $E = 10000 \text{ cm}^{-1}$ (dashed black lines).

to the depolarization rates is larger than that of the singlet component for small j whereas for levels with large j values the singlet contribution is a bit larger than the triplet contribution. It is also interesting to remark that the depolarization rates for different temperatures converge as j increases.

In Table 1, we present fits of the singlet and triplet contribution to the destruction of circular ($k = 1$) and linear ($k = 2$) polarization rates for various temperatures. These variation laws give results with precision better than 10% up to $j = 40.5$. Our results could be implemented in numerical codes concerned with the simulations of the scattering polarization to obtain accurately the magnetic field in the quiet Sun. We note here that both the singlet and triplet contributions to the depolarization rates exhibit a very mild oscillatory behavior on top of their decreasing behavior with increasing j . However, as shown in Table 1, the behavior of all the singlet and some of the triplet depolarization rates can be described by simple power laws within the intended accuracy.

4.3 Comparison between the singlet and triplet contributions

From the above results, one can see that the contributions of the singlet and triplet components of the potential to the depolarization and transfer of polarization cross-sections are not very different from each other despite the vast difference between the singlet and triplet interaction potentials. To investigate this point, we begin by identifying the radial range to which cross-sections are most sensitive for each of the two potential components. To do so, we add an isotropic local perturbation to the interaction potential $V(R, \theta)$, and thus $V(R, \theta)$

Table 1. Depolarization rates ($\times 10^{-10} n_H s^{-1}$) as functions of j .

T (K)	k	$D^k(j)$ [Singlet]	$D^k(j)$ [Triplet]
2000	1	$\frac{0.580672}{j^{0.659399}} - \frac{j^{5.34649}}{4.664955 \times 10^{11}}$	$\frac{1.93722 \sin(0.716361j)}{j^{3.05797}} + \frac{98.9513 \sin(0.034423j)}{j^{2.54382}} - \frac{15.2373 \sin(0.285721j)}{j^{3.25848}}$
	2	$\frac{1.20891}{j^{0.651866}} - \frac{j^{5.45485}}{3.564565 \times 10^{11}}$	$\frac{105.145 \sin(0.0421442j)}{j^{2.28329}} - \frac{2.11805 \sin(1.08345j)}{j^{3.43576}} - \frac{j^{28.7795} \sin(0.763456j)}{1.558629 \times 10^{49}} - \frac{5.8483 \sin(0.29407j)}{j^{2.63312}}$
3000	1	$\frac{0.709969}{j^{0.686909}} - \frac{j^{4.42095}}{1.595641 \times 10^9}$	$\frac{15213.3}{j^{0.29214}} - \frac{27200.8}{j^{0.290325}} + \frac{11988.5}{j^{0.28806}}$
	2	$\frac{952.546}{j^{0.433596}} - \frac{951.134}{j^{0.433343}}$	$\frac{52.7609 \sin(0.053414j)}{j^{1.99877}} + \frac{0.10963 \sin(0.589314j)}{j^{1.44464}} - \frac{j^{30.3895} \sin(0.767695j)}{2.862860 \times 10^{51}} - \frac{1.94657 \sin(1.1667j)}{j^{3.4203}}$
4000	1	$\frac{0.81136}{j^{0.699613}} - \frac{j^{3.42274}}{6.966464 \times 10^8}$	$\frac{21010.6}{j^{0.339994}} - \frac{37614.6}{j^{0.338475}} + \frac{16605.2}{j^{0.336582}}$
	2	$\frac{1309.16}{j^{0.414439}} - \frac{1307.57}{j^{0.414214}}$	$\frac{68.5569 \sin(0.0463297j)}{j^{2.00335}} - \frac{1.80188 \sin(1.25799j)}{j^{3.02838}}$
5000	1	$\frac{0.892242}{j^{0.701794}} - \frac{j^{2.31421}}{4.513851 \times 10^6}$	$\frac{893.269}{j^{0.584877}} - \frac{892.011}{j^{0.584538}}$
	2	$\frac{1613.83}{j^{0.401726}} - \frac{1612.08}{j^{0.401517}}$	$\frac{80.6866 \sin(0.0425921j)}{j^{2.00046}} - \frac{1.8668 \sin(1.27448j)}{j^{2.94507}}$
6000	1	$\frac{0.957088}{j^{0.694838}} - \frac{j^{1.41925}}{1.37194 \times 10^4}$	$\frac{1111.39}{j^{0.596797}} - \frac{1110.04}{j^{0.59651}}$
	2	$\frac{1629.84}{j^{0.392947}} - \frac{1627.96}{j^{0.39272}}$	$\frac{94.2274 \sin(0.0391989j)}{j^{2.00339}} - \frac{1.97187 \sin(1.27964j)}{j^{2.90373}}$
7000	1	$\frac{1.01366}{j^{0.685892}} - \frac{j^{0.999696}}{7.41299 \times 10^4}$	$\frac{36.7084 \sin(0.0453646j)}{j^{1.99647}} - \frac{0.412163 \sin(1.60238j)}{j^{2.30586}}$
	2	$\frac{1962.72}{j^{0.386759}} - \frac{1960.73}{j^{0.386556}}$	$\frac{109.44 \sin(0.0360508j)}{j^{2.00927}} - \frac{2.09951 \sin(1.27903j)}{j^{2.88506}}$
8000	1	$\frac{1.06554}{j^{0.679555}} - \frac{j^{0.838967}}{1.50584 \times 10^3}$	$\frac{41.3965 \sin(0.0426049j)}{j^{2.0026}} - \frac{0.435909 \sin(1.59865j)}{j^{2.29474}}$
	2	$\frac{2060.22}{j^{0.382413}} - \frac{2058.13}{j^{0.382207}}$	$\frac{126.848 \sin(0.0330478j)}{j^{2.01682}} - \frac{2.24232 \sin(1.27506j)}{j^{2.8798}}$
9000	1	$\frac{1.11331}{j^{0.676387}} - \frac{j^{0.804209}}{1.85496 \times 10^3}$	$\frac{46.5176 \sin(0.0399658j)}{j^{2.0099}} - \frac{0.462707 \sin(1.59339j)}{j^{2.29394}}$
	2	$\frac{2117.99}{j^{0.379395}} - \frac{2115.8}{j^{0.379184}}$	$\frac{147.34 \sin(0.030095j)}{j^{2.02545}} - \frac{2.39696 \sin(1.26892j)}{j^{2.88306}}$
10000	1	$\frac{1.15734}{j^{0.675571}} - \frac{j^{0.841397}}{1.70383 \times 10^3}$	$\frac{172.447 \sin(0.0270968j)}{j^{2.03482}} - \frac{2.56193 \sin(1.26123j)}{j^{2.89201}}$
	2	$\frac{2407.5}{j^{0.37736}} - \frac{2405.22}{j^{0.377167}}$	$\frac{148.979 \sin(0.0300641j)}{j^{2.01433}} - \frac{1.30349 \sin(1.70308j)}{j^{2.77411}} - \frac{0.591264 \sin(1.26576j)}{j^{1.8358}} - \frac{0.262735 \sin(0.985727j)}{j^{1.3754}}$
11000	1	$\frac{1.19809}{j^{0.676055}} - \frac{j^{0.925462}}{1.29377 \times 10^3}$	$\frac{2.03058 \sin(0.575704j)}{j^{2.47863}} + \frac{25.1946 \sin(0.0549002j)}{j^{1.82949}} + \frac{j^{27.0852} \sin(0.689243j)}{4.025176 \times 10^{46}} - \frac{1.56857 \sin(1.22555j)}{j^{3.63018}}$
	2	$\frac{2129.78}{j^{0.376117}} - \frac{2127.42}{j^{0.375892}}$	$\frac{6.24505 \sin(0.444197j)}{j^{2.6285}} + \frac{79.9193 \sin(0.0429266j)}{j^{1.87806}} - \frac{5.34946 \sin(0.979811j)}{j^{3.43624}}$
12000	1	$\frac{1.23592}{j^{0.676985}} - \frac{j^{1.04281}}{8.61328 \times 10^4}$	$\frac{2.35808 \sin(0.562536j)}{j^{2.52625}} + \frac{26.0198 \sin(0.0539131j)}{j^{1.82608}} + \frac{j^{35.9765} \sin(0.84497j)}{2.084109 \times 10^{60}} - \frac{1.73953 \sin(1.20264j)}{j^{3.63959}}$
	2	$\frac{2269.39}{j^{0.375461}} - \frac{2266.96}{j^{0.375244}}$	$\frac{200.538 \sin(0.0245231j)}{j^{2.03363}} - \frac{1.43117 \sin(1.70595j)}{j^{2.80279}} - \frac{0.676838 \sin(1.26708j)}{j^{1.8719}} - \frac{0.332371 \sin(0.980758j)}{j^{1.42887}}$
13000	1	$\frac{1.27101}{j^{0.677788}} - \frac{j^{1.18463}}{5.2231 \times 10^4}$	$\frac{2.81554 \sin(0.548392j)}{j^{2.59105}} + \frac{26.398 \sin(0.0533797j)}{j^{1.81963}} - \frac{j^{32.1112} \sin(0.766856j)}{3.0086945 \times 10^{54}} - \frac{1.98032 \sin(1.1719j)}{j^{3.6541}}$
	2	$\frac{2409.81}{j^{0.375299}} - \frac{2407.31}{j^{0.37509}}$	$\frac{82.1085 \sin(0.0420508j)}{j^{1.86367}} - \frac{1.79062 \sin(1.21992j)}{j^{3.34602}} + \frac{10.8506 \sin(0.416841j)}{j^{2.84112}} - \frac{5.60116 \sin(0.856063j)}{j^{3.29195}}$
14000	1	$\frac{1.30339}{j^{0.678139}} - \frac{j^{1.344}}{2.96907 \times 10^4}$	$\frac{3.31323 \sin(0.533883j)}{j^{2.64882}} + \frac{26.7466 \sin(0.0527932j)}{j^{1.81369}} - \frac{j^{32.483} \sin(0.766833j)}{7.050008 \times 10^{55}} - \frac{2.22853 \sin(1.14656j)}{j^{3.66373}}$
	2	$\frac{2169.11}{j^{0.375563}} - \frac{2166.55}{j^{0.375326}}$	$\frac{83.361 \sin(0.0415676j)}{j^{1.8586}} - \frac{2.02322 \sin(1.20303j)}{j^{3.35631}} + \frac{12.9384 \sin(0.404303j)}{j^{2.88833}} - \frac{6.31348 \sin(0.838442j)}{j^{3.30842}}$
15000	1	$\frac{1.3331}{j^{0.677885}} - \frac{j^{1.5146}}{1.62161 \times 10^4}$	$\frac{3.83097 \sin(0.519459j)}{j^{2.69609}} + \frac{27.0655 \sin(0.0521695j)}{j^{1.80817}} + \frac{j^{37.0213} \sin(0.844876j)}{3.493497 \times 10^{62}} - \frac{2.47177 \sin(1.12596j)}{j^{3.67129}}$
	2	$\frac{1956.09}{j^{0.376172}} - \frac{1953.47}{j^{0.375905}}$	$\frac{11.5399 \sin(0.393126j)}{j^{2.75561}} + \frac{84.5611 \sin(0.0413531j)}{j^{1.85581}} + \frac{j^{29.4812} \sin(0.839229j)}{1.978907 \times 10^{50}} - \frac{7.59474 \sin(0.935008j)}{j^{3.46111}}$

is multiplied by a Gaussian magnification factor of the form ¹

$$G(R) = 1. + \exp[-10(R - R_0)^2] \quad (9)$$

where R_0 refers to the center of the Gaussian perturbation. We vary R_0 to scan the entire integration range.

¹ Due to the mild anisotropy present in the potential, one should in principle devise a θ -dependent perturbation which can slightly shift the radial range of sensitivity.

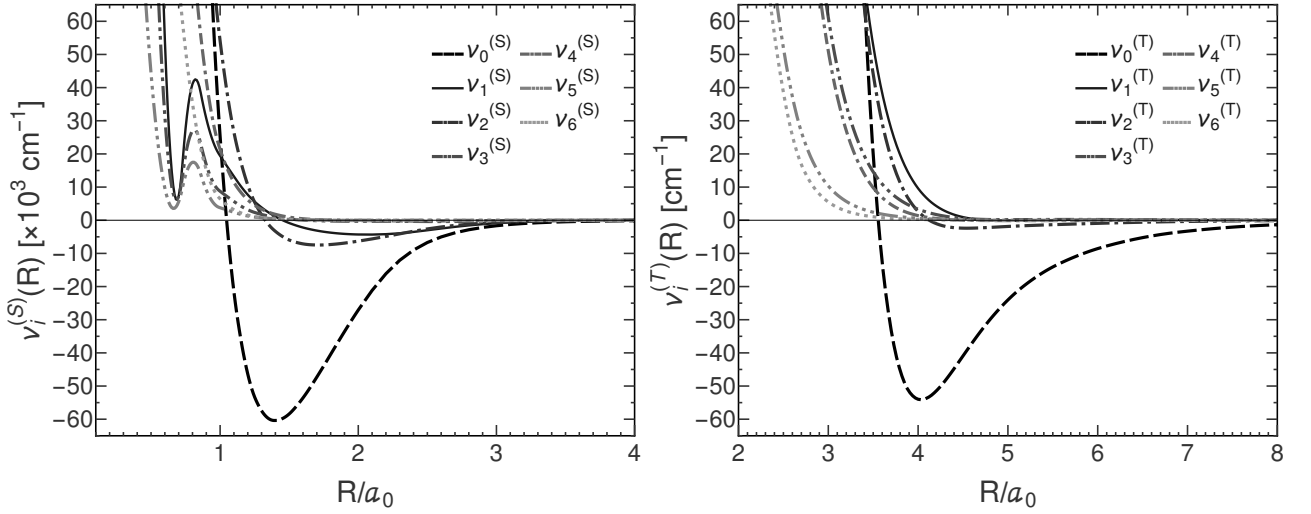


Figure 12. The radial variation of the first seven Legendre coefficients of the singlet (left panel) and triplet (right panel) components of the potential. Note that the potential well depth of $V_{\lambda=0}^{(S)}$ is a factor of $\sim 10^3$ greater than the well depth of $V_{\lambda=0}^{(T)}$.

We find that the total cross-sections calculated with the perturbed potential components differ significantly from those calculated with the unperturbed potential only when $5 \lesssim R_0 \lesssim 11$ for the singlet component and $2 \lesssim R_0 \lesssim 14$ for the triplet component (see Figure 11). As it can be seen from Figure 11, these ranges slightly shift to smaller radial distances as the energy of collision increases. We note here that for the triplet part of the potential, the radial range where the potential is sensitive to perturbations, is wider compared to that for the singlet component (see Figure 11). By carefully examining the cross-sections calculated with the perturbed and with unperturbed potentials, we find that for the singlet case (the potential component that has a very deep well), the contributions to the cross-sections do not come from the bottom of the well but rather from the part of its far side where the potential starts curving down. This part of the potential is usually called “intermediate region”, since neither close-range distances nor long-range distances are contained in this region. Interestingly, in the intermediate region of the singlet part of the potential, the difference between the two potential components is not as severe as the difference between the well depth of the two potential components.

Let us expand the potential in the basis of Legendre polynomials,

$$V^{(i)}(R, \theta) = \sum_{\lambda=0}^{\infty} V_{\lambda}^{(i)}(R, \theta) = \sum_{\lambda=0}^{\infty} \mathcal{V}_{\lambda}^{(i)}(R) P_{\lambda}(\cos \theta) \quad (10)$$

where

$$\mathcal{V}_{\lambda}^{(i)}(R) = \int_{-1}^1 d(\cos \theta) V^{(i)}(R, \theta) P_{\lambda}(\cos \theta), \quad (11)$$

Table 2. Scattering cross-sections $\sigma(0 \rightarrow L)$ in \AA^2 , for collision energy $E = 5000 \text{ cm}^{-1}$.

$\sigma(0 \rightarrow L)$	$V_0^{(S)}$	$V_0^{(T)}$	$V_1^{(S)}$	$V_1^{(T)}$	$V_2^{(S)}$	$V_2^{(T)}$	$V_3^{(S)}$	$V_3^{(T)}$	$V_4^{(S)}$	$V_4^{(T)}$	$V_5^{(S)}$	$V_5^{(T)}$	$V_6^{(S)}$	$V_6^{(T)}$
$L = 0$	131.85	71.709	39.806	24.203	31.213	24.013	7.144	13.382	6.153	13.097	3.906	1.553	4.256	1.110
$L = 1$	0.000	0.000	6.555	5.306	2.874	0.000	0.301	0.727	0.012	0.000	0.034	0.049	0.000	0.000
$L = 2$	0.000	0.000	3.592	3.046	6.097	5.203	0.545	0.355	0.310	0.784	0.066	0.149	0.101	0.162
$L = 3$	0.000	0.000	2.553	2.211	3.346	0.000	9.184	5.023	0.007	0.000	0.138	0.203	0.000	0.000
$L = 4$	0.000	0.000	1.883	1.762	3.161	2.990	0.417	0.383	3.563	4.718	0.031	0.046	0.158	0.177
$L = 5$	0.000	0.000	1.393	1.474	1.387	0.000	0.389	0.774	0.005	0.000	1.157	3.518	0.000	0.000
$L = 6$	0.000	0.000	1.290	1.269	2.040	2.143	1.521	1.805	0.343	0.724	0.038	0.034	0.906	3.099
$L = 7$	0.000	0.000	1.039	1.115	4.411	0.000	0.174	0.288	0.005	0.000	0.140	0.215	0.000	0.000
$L = 8$	0.000	0.000	0.867	0.994	1.526	1.681	0.215	1.010	0.378	1.983	0.035	0.049	0.159	0.167
$L = 9$	0.000	0.000	0.900	0.894	1.451	0.000	0.208	0.630	0.004	0.0000	0.046	0.077	0.000	0.000
$L = 10$	0.000	0.000	0.910	0.811	1.236	1.384	0.041	0.162	0.276	0.877	0.392	0.520	0.088	0.090
$L = 11$	0.000	0.000	0.769	0.740	1.536	0.000	0.196	0.987	0.007	0.000	0.024	0.042	0.000	0.000
$L = 12$	0.000	0.000	0.592	0.677	0.860	1.173	0.083	0.222	0.111	0.869	0.148	0.113	0.289	0.411

and separately study the effect of each term on the collision process while ignoring the interference between different potential terms. In Equations 10 and 11, $i = S, T$ refers to the singlet and triplet components respectively. Figure 12 shows the radial dependence of the first seven coefficients of the potential expansion in terms of Legendre functions for the singlet (left panel) and triplet (right panel) parts. As can be seen, the depths of the potential wells drastically decrease with increasing λ . Further the difference between the Legendre coefficients of the singlet and triplet potential components drastically decreases as λ increases.

Separately feeding the different potential terms $V_\lambda^{(i)}(R, \theta)$ to MOLSCAT while fixing the energy of collisions to $E = 5000 \text{ cm}^{-1}$, we obtain the cross-sections $\sigma(0 \rightarrow L)$, which we show in Table 2.

It can be seen from Table 2 that the components $V_0^{(S,T)}$, which contribute the most to the depth of the potential well, contribute only to $\sigma(0 \rightarrow L=0)$ and do not lead to any rotational excitation of the CN molecule [i.e. they do not contribute to $\sigma(0 \rightarrow L > 0)$] due to their isotropic nature. It can also be noticed that for almost all $V_\lambda^{(S,T)}$'s, the largest contribution goes to the $\sigma(0 \rightarrow L=0)$ channel. In this particular channel, the singlet contribution is significantly larger than the contribution of the triplet component of the potential for the first few $V_\lambda^{(i)}$ Legendre terms. For example, the singlet cross-section is roughly 85% larger than the triplet cross-section for the $\lambda = 0$ term, which reflects the difference between $V_0^{(S)}$ and $V_0^{(T)}$. Nevertheless, the difference between the singlet and the triplet contributions to

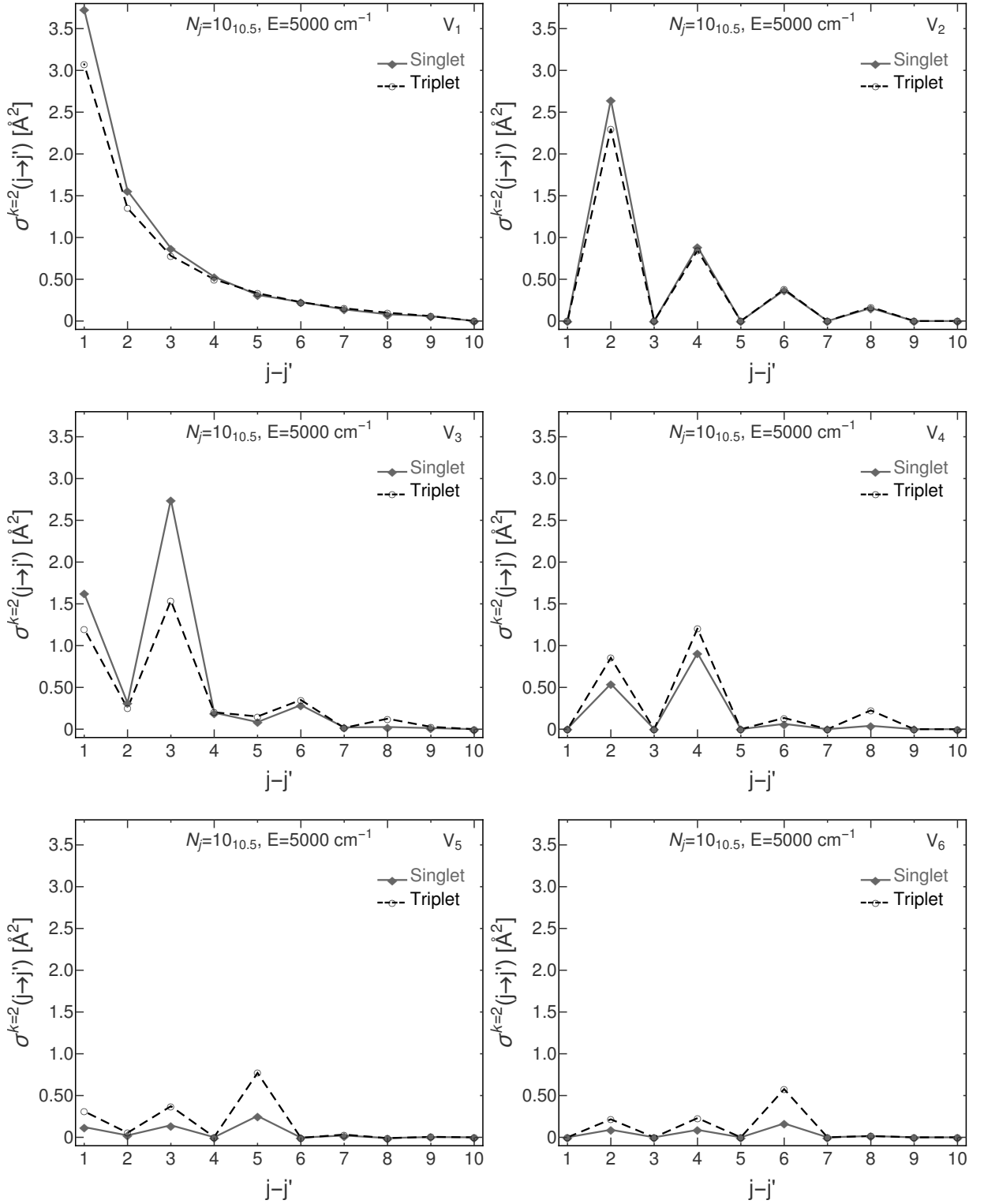


Figure 13. Contributions of the different Legendre terms, $V_\lambda^{(S,T)}$, ($\lambda = 1, 2, \dots, 6$), of the singlet (solid gray lines) and triplet (dashed black lines) components of the potential to the transfer of polarization cross-sections for the level $N_j = 10_{10.5}$ and $k = 2$.

the $\sigma(0 \rightarrow L=0)$ channel decreases as the difference between the two potential components decreases with increasing λ . We also note that for the channels with $L > 0$, the cross-sections $\sigma(0 \rightarrow L)$ are almost generally much smaller than the corresponding $\sigma(0 \rightarrow L=0)$. Moreover, for a given $V_\lambda^{(S,T)}$ term, the cross-sections are relatively large when $L = m\lambda$ with m being an integer. These cross-sections tend to decrease as L increases. Furthermore, the difference between the singlet and triplet cross-sections for a given λ tends to decrease as L increases.

Now since $\sigma(0 \rightarrow L=0)$ does not contribute to depolarization nor transfer of polarization cross-sections, only the $\sigma(0 \rightarrow L > 0)$ arising from the less-different Legendre terms $V_{\lambda>0}^{(S)}$ and $V_{\lambda>0}^{(T)}$ contribute to the depolarization and transfer of polarization cross-sections. This explains why the singlet and triplet depolarization and transfer of polarization rates are not very different from each other despite the vast difference between the singlet and triplet components of the potential.

Figure 13 compares the contributions to the transfer of polarization for the level $N_j = 10_{10.5}$ from the first six Legendre terms of the singlet potential terms, $V_\lambda^{(S)}$, ($\lambda = 1, 2, \dots, 6$), to the corresponding triplet ones, $V_\lambda^{(T)}$, ($\lambda = 1, 2, \dots, 6$), as functions of $\Delta j = j - j'$ and for the collision energy, $E = 5000 \text{ cm}^{-1}$ ². It can be concluded that the singlet and triplet contributions are not very different from each other.

5 SOLAR IMPLICATIONS

Let us now briefly consider the implication of our results for the solar CN molecule. To estimate the effect of isotropic collisions, we compare the collisional depolarization rates D^2 of the CN ground state ($X^2\Sigma$), for typical photospheric Hydrogen density ($n_H = 10^{15} - 10^{16} \text{ cm}^{-3}$), to the inverse lifetime ($=\frac{1}{t_{life}}$) of the lower levels of some representative lines. We show that the rates D^2 dominate the radiative rates for $n_H = 10^{16} \text{ cm}^{-3}$ and thus all rotational levels of the lower electronic state $X^2\Sigma$ are linearly depolarized. We notice that $\frac{1}{t_{life}} = B_{lu}I(\lambda)$, where $B_{lu} = (g_u/g_l)(c^2/2h\nu_{ul}^3)A_{ul}$ denotes the Einstein coefficient for absorption; A_{ul} is the transition probability per unit time for spontaneous emission, g_u and g_l are the statistical weights of upper and lower levels, h is the Planck's constant and c is the velocity of light. In addition,

$$I(\lambda) = I_{min}(\lambda)I_c(\lambda) \quad (12)$$

² Here we do not show the contribution of the isotropic Legendre terms $V_0^{(S,T)}$ as they are identically zero.

Table 3. Comparison between the linear depolarization rates D^2 of the CN $X^2\Sigma$ state to its inverse lifetime $\frac{1}{t_{life}} = B_{\ell u}I(\lambda)$. We also compare the $B_{\ell u}I(\lambda)$ with the values $(\omega_L|g_{j_\ell}|)^{-1}$ which estimate the Hanle depolarization.

λ (Å)	I_{min}	I_c ($10^{-5}\text{erg cm}^{-2}$ $\text{s}^{-1}\text{sr}^{-1}\text{Hz}^{-1}$)	$A_{u\ell}$ (10^6s^{-1})	$B_{\ell u}I(\lambda)$ (s^{-1})	$\omega_L g_{j_\ell} $ (10^3s^{-1})		j_ℓ	$D^{k=2}(j)$ (s^{-1})	
					B=10G	B=100G		$n_H = 10^{15}\text{cm}^{-3}$	$n_H = 10^{16}\text{cm}^{-3}$
3839.136	0.1920	1.0462	7.0401	2014.16	2286.5	22865	37.5	7864.13	78641.3
3850.178	0.1707	1.0479	6.9783	1793.18	2981.2	29812	27.5	12359.3	123593
3862.692	0.6564	1.0497	7.0958	7092.58	1231.2	12312	72.5	2446.76	24467.6
3870.871	0.2097	1.0510	7.0811	2278.23	1407.1	14071	62.5	3228.44	32284.4
3871.372	0.1425	1.0510	6.3860	1396.82	13502.9	135029	4.5	79432.9	794329
3879.707	0.3365	1.0523	7.0592	3674.10	1890.7	18907	46.5	5491.44	54914.4
3880.681	0.2635	1.0524	7.2926	2974.96	7650.9	76509	11.5	32029.9	320299
3880.784	0.2763	1.0524	7.0763	3027.07	2022.6	20226	43.5	6156.94	61569.4
3883.114	0.1568	1.0528	7.1339	1675.55	3904.6	39046	22.5	15886.1	158861

is the line intensity with $I_{min}(\lambda)$ being the relative intensity of the line center and I_c being the absolute continuum intensity at disk center.

In Table 3, we show some selected lines of the $B^2\Sigma - X^2\Sigma$ system of CN along with the corresponding values of radiative excitation rates, $B_{\ell u}I(\lambda)$, and the linear depolarization rates, $D^{k=2}(j_\ell)$, calculated at the effective photospheric temperature, $T_{\text{eff}} = 5778$ K, and at typical values of Hydrogen density $n_H = 10^{15}\text{cm}^{-3}$ and $n_H = 10^{16}\text{cm}^{-3}$ in the photosphere. The relative intensity of the absorption lines are taken from the solar atlas of Delbouille et al. (1972) whereas the corresponding absolute continuum values are interpolated from the data given in (Allen & Cox 1999). The values of the Einstein A coefficients, Landé factors g_{j_ℓ} and j_ℓ are taken from Berdyugina (2009, private communication).

It is obvious that for $n_H = 10^{16}\text{cm}^{-3}$ all the rotational levels of the CN $X^2\Sigma$ state are linearly depolarized since $D^{k=2}(j_\ell, n_H = 10^{16}\text{cm}^{-3}) \gg B_{\ell u}I(\lambda)$. This is also true in the case $n_H = 10^{15}\text{cm}^{-3}$ especially for rather small j_ℓ ; however, for sufficiently large j_ℓ the radiative excitation and linear depolarization rates of the CN $X^2\Sigma$ state are comparable. Hence one has to take into account the depolarization rates when solving the statistical equilibrium equation for the polarization of observed lines.

We also consider the effect of the photospheric turbulent magnetic field on the polarization of the CN ground state, $X^2\Sigma$. It is well known that the polarization is sensitive to Hanle depolarization only if the magnetic field value is around a critical value B_c (more precisely the magnetic field has a value in the window $\sim 0.1B_c - 10B_c$). In other words, Hanle effect is relevant if the time-life of the level under consideration [$\sim (B_{\ell u}I)^{-1}$ for the ground state] is of order $(\omega_L|g_{j_\ell}|)^{-1}$ where $\omega_L = 8.79 \times 10^6 B$ denotes Larmor angular frequency with B being the magnetic field strength in Gauss.

In Table 3, we show the values of $\omega_L|g_{j_\ell}|$ calculated at $B = 10\text{G}$ and $B = 100\text{G}$. It is

clear that $\omega_L |g_{j_\ell}| \gg B_{\ell u} I$ in all cases. Therefore, for typical values of the turbulent magnetic field $\sim 10 - 100$ G, Hanle effect is not efficient for the CN ground state, CN $X^2\Sigma$. CN $X^2\Sigma$ is sensitive to the Hanle effect of very weak magnetic field strength since it is a long lived level and thus the saturation regime of the Hanle effect on its linear polarization is quickly attempted.

6 CONCLUSION

The so-called second solar spectrum (SSS) of the CN molecule is the observational signature of the polarization of the CN states (see, e.g., Trujillo Bueno et al. 2004, Landi Degl'Innocenti & Landolfi 2004). Molecular lines arising from transitions between rotational levels can be depolarized by collisions but also by the Hanle effect due to the presence of solar magnetic fields. Therefore, information about Hanle and collisional effects are mixed in the same observable (the polarization state), which makes the interpretation of the observed polarization in terms of magnetic fields very complicated in the absence of collisional data.

In this paper we provide depolarization and polarization transfer rates of the $X^2\Sigma$ state of the CN due to collisions with neutral hydrogen in its ground state 2S . These rates would be useful to interpret CN violet lines in the second solar spectrum in terms of solar magnetic field (Shapiro et al. 2011). A detailed discussion of the results is presented we obtain useful variation laws of the polarization transfer rates with the temperature and the angular momentum j . Solar implications of our results are discussed.

ACKNOWLEDGEMENTS

M.D. wishes to thank the *Université Le Havre Normandie* for their kind invitation and hospitality. Results of *ab initio* calculations have been obtained under support of the RSF grant No. 17-12-01395. Y.K. also acknowledges the partial support from RFBR grant No. 18-05-00119.

REFERENCES

- Allen C. W., & Cox A. N. (1999). *Allen's Astrophysical quantities*. New York: AIP Press.
- Asensio Ramos A. & Trujillo Bueno J., 2005, *ApJ Letters*, 635, 109
- Berdyugina S.V., 2009, private communication
- Berdyugina S.V. & Fluri D., 2004, *A&A*, 417, 775
- Corey G. C. & Alexander M., 1985, *The Journal of Chemical Physics*, 83, 5060

- Corey G. C. & Smith, A. D., 1985, *The Journal of Chemical Physics*, 83, 5663
- Corey G. C., Alexander M., & Dagdigan P.J., 1986, *The Journal of Chemical Physics*, 84, 1547
- Dagdigan P. & Alexander M., 2009, *The Journal of chemical physics*, 130, 164315
- Davidson E. R. & Silver D. W., 1977, *Chem. Phys. Lett.*, 52, 403
- Delbouille L., Roland G., & Neven L. 1972, *Photometric atlas of the solar spectrum from $\lambda = 3000$ to $\lambda = 10000$* , Université de Liège, Institut d'Astrophysique (ed.)
- Derouich M., Sahal-Bréchet S., Barklem P. S. & O'Mara B. J., 2003, *A&A*, 404 (2), 763
- Derouich M., 2006, *A&A*, 449, 1
- Derouich M., Trujillo Bueno J., Manso Sainz R., 2007, *A&A*, 472, 269
- Dunning T. H., 1989, *J. Chem. Phys.*, 90, 1007
- Faurobert M. & Arnaud J., 2003, *A&A*, 412, 555
- Flower D., 1990, *Molecular Collisions in the Interstellar Medium* (Cambridge University Press: Cambridge)
- Gandorfer A., 2000, *The Second Sol. Spectrum: A high spectral resolution polarimetric survey of scattering polarization at the solar limb in graphical representation, Vol. 1: 4625 to 6995* (Hochschulverlag AG an der ETH Zurich)
- Goldflam R., Green S., Kouri D. J., 1977, *J. Chem. Phys.*, 67, 4149
- Hutson J.M. & Green S., MOLSCAT computer code, version 14 (1994) distributed by Collaborative Computational Project No. 6 of the Engineering and Physical Sciences Research Council (UK).
- Landi Degl'Innocenti E. & Landolfi, M. 2004, *Polarization in Spectral Lines* (Dordrecht: Kluwer)
- Lique F., Spielfiedel A. & Feautrier N., 2007, *Journal of Physics B: Atomic, Molecular, and Optical Physics*, 40, 787
- Milić I. & Faurobert M., 2012, *A&A*, 547, 7
- Mohan Rao D., & Rangarajan K. E., 1999, *ApJ*, 524, L139
- Roueff E. & Lique F., 2013, *Chemical Reviews*, 113, 8906
- Sahal-Bréchet S., 1977, *ApJ.*, 213, 887
- Shapiro A. I., Fluri D. M., Berdyugina S. V., Bianda M., Ramelli R., 2011, *A&A*, 529, A139
- Trujillo Bueno J., 2002, *Atomic Polarization and the Hanle Effect*, arXiv:astro-ph/0202328
- Trujillo Bueno J., Shchukina N. & Asensio Ramos A, 2004, *Nature*, 430, 326
- Wener H.-J., Knowles P. J., 1988, *J. Chem. Phys.*, 89, 5803
- Werner H.-J., Knowles P. J., Knizia G., Manby F. R., Schütz M. et al., MOLPRO, version 2010.1, a package of ab initio programs, 2010, see <http://www.molpro.net>
- Williams H. L., Mas E. M., Szalewicz K. & Jeziorski B., 1995, *The Journal of Chemical Physics*, 103, 7374
- Yang B., Wang X. H., Stancil P. C., Bowman J. M., Balakrishnan N. & Forrey R. C., 2016, *J. Chem. Phys.*145, 224307